RSC Advances

PAPER

View Article Online
View Journal | View Issue

Cite this: *RSC Adv.*, 2019, **9**, 15542

CO_2-philic moderate selective layer mixed matrix membranes containing surface functionalized NaX towards highly-efficient CO_2 capture†

Mohammad Salehi Maleh and Ahmadreza Raisi *

A functional moderate selective layer mixed matrix membrane (F-MSL-MMM) is a promising candidate to obtain superior separation of industrial gases, compared to commonly mixed matrix membranes. In this work, highly permeable and selective F-MSL-MMMs consisting of a moderate Pebax layer filled with functionalized NaX nano-zeolite over a microstructure PES support layer with the desired operating stability were prepared to investigate the effect of –COOH surface functionalization on the NaX nano-zeolites and to achieve the efficient separation of CO_2/N_2, CO_2/CH_4 and CH_4/N_2 gas mixtures. It was found that modification of the nano-zeolite had significant effects on the morphology and gas separation performance of the F-MSL-MMMs. The incorporation of NaX–COOH nano-zeolites into the polymeric matrix showed superior dispersion, capabilities and interactions over unmodified zeolite without any defects. In addition, based on gas permeation results at various filler loadings and feed pressures, different trends were observed for the permeability and selectivity of the F-MSL-MMMs. Combination of NaX up to 1.5% into the moderate selective layer enhanced the CO_2 permeability (187.76 barrer) and CO_2/N_2 (288.86), CO_2/CH_4 (57.41) and N_2/CH_4 (5.03) selectivities at 6 bar.

Received 5th March 2019
Accepted 6th May 2019

DOI: 10.1039/c9ra01654f

rsc.li/rsc-advances

Introduction

During the past few decades, the use of polymeric membranes has expanded in gas separation applications, such as CO_2 separation from natural gas and flue gas.[1] Later, a lot of research was performed to improve the properties of polymeric membranes, and as a result, in order to use the advantages of polymeric and inorganic materials, mixed matrix membranes (MMMs) containing a dispersed inorganic phase in a continuous polymer phase were introduced.[2,3] Zeolites are a promising inorganic phase for use in MMMs for gas separation due to their high porosity, superior chemical and thermal stability, uniform pores with molecular sieving property and adsorption selectivity. Likewise, zeolites are particularly effective in CO_2 capture with an absorption-based separation property.[4]

In addition, conventional MMMs have a number of defects that challenge the performance of these membranes. Incompatibility, weak adhesion or repulsion between the polymer and inorganic filler, the hardening of a layer of polymer around the filler, partial pore blockage of porous fillers and particle accumulation result in the creation of various interfacial defects and a non-ideal morphology in the MMMs. In order to fabricate defect-free MMMs, various methods have been widely used by researchers, among which the use of copolymers such as polyether-*block*-amide is one effective solution.[5–7] Polyether-*block*-amide is a rubbery copolymer with the commercial name of Pebax, which includes a rigid polyamide (PA6 or PA12) segment and a soft polyethylene oxide (PEO) segment, the hard-soft structure improving adhesion between the polymer phase and the particles. In addition, the hard polyamide parts provide the mechanical strength of the membranes and the soft polyethylene oxide parts due to their CO_2-philic structure, cause an increase in permeability and selectivity for CO_2 separation from natural gas and flue gas.[2,8]

The surface chemical modification of the filler particles is another effective solution to prevent undesirable spaces near the polymer–particle interface and to avoid the accumulation of fillers, which improves the gas separation performance of MMMs. The filler particles are usually modified by amine, hydroxylic, alkylic, sulfonic acid, carboxylic acid or imidazole groups.[9] Up to now, various filler particles, such as SiO_2, CNTs, MCM-41, ZIF-8, MOFs or GO,[2,3,8,10–18] have been modified and used as a dispersant phase in a polymeric matrix to improve the membrane separation properties.

Among the various functional groups, the effect of modification of nano-zeolites with carboxylic functional groups in a moderate selective layer has not been studied, while this functional group can have very favorable effects on the performance of functional moderate selective layer mixed matrix membranes (F-MSL-MMMs). The existence of carboxylic

Department of Chemical Engineering, Amirkabir University of Technology (Tehran Polytechnic), Hafez Ave., P. O. Box 15875-4413, Tehran, Iran. E-mail: raisia@aut.ac.ir; Fax: +98 21 66405847; Tel: +98 21 64543125

† Electronic supplementary information (ESI) available. See DOI: 10.1039/c9ra01654f

functional groups in F-MSL-MMMs materials has also been confirmed to enhance their gas separation performance due to a reversible reaction with CO_2.[19] The surface chemical modification of the fillers enables them to react reversibly with CO_2, and, therefore, they are expected to act as carriers for CO_2. The surface modification of fillers with carboxylic groups develops not only a filler–polymer interface compatibility but also improves the selectivity and permeability of CO_2. The F-MSL-MMMs including modified fillers are expected to overcome Robeson's upper limit and have greater stability and mechanical strength. Consequently, the main aim of this study is to investigate the effect of chemical modification on improving the morphology of the Pebax–NaX nano-zeolite interface, avoiding the accumulation of nanoparticles, as well as improving permeability and selectivity. In addition, a further goal is a comparison of the performance of MSL-MMMs containing NaX and NaX–COOH nanoparticles.

In this work, MSL-MMMs containing pure and modified NaX nanoparticles were fabricated separately in four loadings in a Pebax-1657 polymeric matrix on polyethersulfone (PES) sublayer membranes. The MSL-MMMs were characterized by SEM, FTIR, DSC and contact angle (CA) analyses. The NaX nano-zeolites were synthesized by a hydrothermal method, and then functionalized with carboxylic groups by the reflux method. The crystallinity structure, crystal size, particle size, particle shape and chemical properties of the nanoparticles were characterized by XRD, FESEM, FTIR, BET and DLS analyses. The effect of filler surface modification, loading of filler and operating conditions, such as feed pressure and long-term stability, on the permeability of pure CO_2, CH_4, and N_2 gases, as well as the CO_2/N_2, CO_2/CH_4 and CH_4/N_2 gas selectivities of MSL-MMMs, were studied.

Experimental

Materials

Ethanol (EtOH), methanol (MeOH), *N*,*N*-dimethyl-formamide (DMF), sodium hydroxide (NaOH) and chloroacetic acid (ACS, reagent) were purchased from Merck (Germany). Sodium aluminate ($NaAlO_2$) and fumed silica (SiO_2, 7 nm) were purchased from Sigma-Aldrich (USA). Pebax® MH 1657 (a copolymer with a combination of PA6 and PEO oxide with a weight ratio of 40/60) and PES (MW = 58 000 g mol^{-1}, Ultrason E6020P) were purchased from Arkema Inc. (France) and BASF (Germany), respectively. In all experiments, deionized water (DI) was used. All chemicals with a purity higher than 99% were used without further purification. Furthermore, CO_2, CH_4 and N_2 gases with a purity > 99.999% were used in the permeation experiments.

Synthesis and functionalization of NaX nano-zeolite

The synthesis of NaX nano-zeolites was performed by the hydrothermal heating method using a microwave oven, according to the procedure previously presented by Ansari *et al.*[20] In this process, first, 5.34 g of NaOH was added to a polypropylene bottle containing 50 g of DI water, and when it was completely dissolved, the solution temperature increased. After cooling the solution to the ambient temperature and adding 2.42 g of $NaAlO_2$, the solution became milky and then became colorless again after a few moments of continuous stirring. Then, 3.43 g of fumed silica was slowly added to the solution. Finally, to obtain a homogeneous alumina silicate gel, the solution was continuously stirred at 25 °C for 24 h. Then, for the hydrothermal heating, the prepared gel was placed in a microwave oven (CE1110C, Samsung, Korea, 900 W output power, wavelength of 2.45 GHz) at 90 °C for 3 h until crystals of NaX zeolite were formed. Then, for the separation and purification of the synthesized NaX nano-zeolite, the resulting solution was initially washed several times using a centrifuge with DI water to remove the unreacted agents and for the pH to be normalized (usually below 8) and then dried in an oven at 80 °C for 24 h.

The NaX nano-zeolites were functionalized by carboxylic groups based on the method provided by Ingole *et al.*[21] First, 1.5 g of NaX was added to 225 mL of DI water and stirred at 25 °C and sonicated for 2 h and 1 h, respectively. Then, 1.925 g of chloroacetic acid was slowly added to the NaX suspension under stirring on a magnetic stirrer. After reflux at around 100 °C for 8 h, the suspension mixture was first cooled to the ambient temperature and then washed using a centrifuge for 10 min with DI water until it reached normal pH. After washing 4 times, it was placed in an oven to dry at 80 °C for 24 h. A schematic of the steps for the synthesis and functionalization of NaX is shown in Fig. S1 in the ESI.†

Fabrication of MSL-MMMs

The PES support sublayer of MSL-MMM was fabricated by the non-solvent phase inversion method.[22] First, in order to prepare a clear homogeneous PES solution, 16 g of the dried PES granules were dissolved in 84 g of DMF solvent and then stirred for 24 h. Finally, the solution was placed under vacuum for 2 h to remove all the air bubbles. Then, using a casting knife with a certain gap (200 μm), a layer of PES polymeric solution was cast on a flat glass plate and immediately placed in a non-solvent bath (DI water at 25 °C) and allowed to exchange the solvent/non-solvent. After enough time, the phase inversion process was complete and the formed PES membrane was immersed in another DI water bath for 24 h, during which the remaining solvent in the membrane was absolutely removed. Then, the PES membrane was dried at ambient temperature for 24 h. Finally, a PES support membrane with a thickness of ~60 μm was obtained.

The MSL-MMMs were prepared by casting of an MSL-MMMs doped solution on the PES sublayer membrane by the solution casting-solvent evaporation method. The casting doping solution included Pebax-1657 polymer, water/ethanol solvent and nano-zeolite particles. Initially, in order to remove humidity, the nanoparticles and copolymer granules were dried in an oven at 60 °C for 5 h. The Pebax-1657 was dissolved in water/ethanol (30/70% by weight) solvent under reflux and stirring at 70 °C for 24 h to obtain a homogeneous Pebax solution. Then, a certain amount of homogenous suspension of nanoparticles in the

water/ethanol (30/70% by weight) solvent was prepared and sonicated for 30 min. In order to prepare the doping solution containing nanoparticles, 1/4 of the prepared homogeneous polymer solution was added in 4 steps, each time, to the homogenous suspension, stirred for 30 min and sonicated for 15 min. The final solution was stirred vigorously for 60 min and placed in an ultrasonic bath for 30 min. The weight percentage of each component of the doping solution for the preparation of different membranes is listed in Table 1. To fabricate an MSL-MMM, the PES sublayer was first fixed on a piece of flat glass *via* removable tape and then using a casting-knife with a certain gap (350 μm), a layer of doping solution was cast onto the PES substrate layer. For the solvent evaporation, the prepared films were placed in an oven at 35 °C for 24 h, and to eliminate the remaining solvent, they were placed in an oven at 60 °C for 12 h. Finally, the thickness of the selective layer was ~15 μm on the PES support layer. A schematic of the procedure for preparing the PES substrate membrane, the doping solution containing nano-zeolite particles and MSL-MMMs is illustrated in Fig. S2.†

Characterization analyses

The crystalline structures of the NaX nano-zeolites were investigated using an X-ray diffraction (XRD) instrument (Equinox 3000, Inel, France). Likewise, the crystallinity degree of the membranes was calculated using the XRD analysis. The XRD tests were carried out using CuKα radiation of $\lambda = 1.5419$ Å at 45 kV, 40 mA, 25 °C and angle diffraction (2θ) from 5 to 40° with 0.03° min^{-1} scanning speed. The average crystal size of the nano-zeolites was calculated using Scherrer's equation (eqn (1)) at major peaks with 2θ of 6 (111), 16 (331) and 27° (642).

$$d = \frac{K\lambda}{\beta \cos \theta} \quad (1)$$

In this equation, d is the average crystal size, K is the shape factor, λ is the X-ray wavelength, β is the line broadening from full width at half maximum (FWHM) and θ is the Bragg angle.

The BET analysis areas of the NaX and NaX–COOH nano-fillers were obtained using nitrogen adsorption–desorption isotherms at 77 K on a Quantachrome Autosorb-1 analyzer (USA). Before testing, the nano-zeolite particles were degassed under vacuum at 120 °C and 10^{-4} Pa for 12 h.

Dynamic light scattering (DLS) analysis was applied to measure the particle size distribution of NaX and NaX–COOH nano-fillers using a Malvern Zetasizer Nano (Malvern Instruments, Worcestershire, England) at 632.8 nm wavelength and 173° scattering angle. The samples were dispersed in a water/ethanol mixture by sonication at 20 °C for 1 h before carrying out the DLS analysis.

The presence of functional groups on the surface of NaX and NaX–COOH zeolite nanoparticles, neat Pebax-1657 and the interaction between polymer and particles of MSL-MMMs were characterized using Fourier transform infrared (FTIR) analysis. The FTIR tests were accomplished with a Nicolet Nexus 670 spectrometer (Nicolet Instrument Co., Madison, WI, USA) in the wave number range 400 cm^{-1} to 4000 cm^{-1} under ambient conditions and with a spectral resolution of 4 cm^{-1}. A mean of 20 scans from each membrane (each sample: 2 × 4 cm) and each nanoparticle (each sample: about 0.5–1 g) was taken.

The morphology and particle size range of the synthesized zeolite nanoparticles and also the surface and cross-sectional morphologies of the fabricated neat and MSL-MMMs were studied using FESEM (Hitachi S-4700, NJ, USA) and SEM devices (AIS2300C, Seron Technology's, South Korea), respectively. To prepare the cross-section of the membranes, the samples were broken down in liquid nitrogen. Finally, before taking images with the SEM device, all of the samples (nanoparticles, cross-section and surface of the membranes) were coated with a layer of gold using sputtering.

Investigations of the glass transition temperature (T_g) and crystallinity degree of the membranes were performed with differential scanning calorimeter (DSC) analysis. The DSC analysis was conducted with a Mettler-Toledo instrument (Mettler-Toledo Inc., Switzerland). The DSC measurements were operated in the temperature range from −100 to 220 °C using a standard heating–cooling–heating method at a rate of 10 °C min^{-1} under a pure argon atmosphere. The crystallinity degree of the fabricated membranes was calculated using eqn (2).

$$X_{\text{Crystallinity}} = \frac{\Delta H_m}{\Delta H_m^0} \quad (2)$$

In this equation ΔH_m is the melting enthalpy of each segment of polymer (the area of the melting peak in the DSC curves) and ΔH_m^0 is the melting enthalpy of fully crystalline

Table 1 The composition of casting solution used for the fabrication of MSL-MMMs

Sample name	Solvent (% wt)	Polymer (% wt)	Nanoparticles (% wt)	Membrane
PP	90.0	10	0.0	PES/Pebax
PPN0.5	89.5	10	0.5	PES/Pebax–NaX
PPN1	89.0	10	1.0	PES/Pebax–NaX
PPN1.5	88.5	10	1.5	PES/Pebax–NaX
PPN2	88.0	10	2.0	PES/Pebax–NaX
PPNC0.5	89.5	10	0.5	PES/Pebax–NaX–COOH
PPNC1	89.0	10	1.0	PES/Pebax–NaX–COOH
PPNC1.5	88.5	10	1.5	PES/Pebax–NaX–COOH
PPNC2	88.0	10	2.0	PES/Pebax–NaX–COOH

sections of the polymer ($\Delta H^0_{m,PEO} = 166.4$ J g^{-1} and $\Delta H^0_{m,PA} =$ 230 J g^{-1}).[17,23] The total crystallinity of the fabricated membranes was estimated by considering 60% PEO crystallinity and 40% PA crystallinity.[24]

Gas permeability

An examination of the gas permeability of the fabricated membranes was conducted with a gas permeability apparatus that controlled the temperature and pressure. The gas permeability experiments were operated using a constant volume and variable pressure method. In all single gas permeability measurements, pure gases, including N_2, CH_4 and CO_2, were investigated at temperatures of 25 °C and various pressures of 2, 4 and 6 bar. A cross-flow flat plate membrane module with an effective surface area of 12.5 cm^2 was utilized in the gas permeability apparatus and the permeate pressure downstream of the membrane was measured every 0.3 s by a pressure transmitter. After transmitting data to the computer and plotting the variation in measured pressure over time, the pressure-time gradient (dp/dt) was calculated and by inserting it in eqn (3), the permeability of the gas was obtained. Before each test, the membrane and downstream volume of the membrane were vacuumed by a vacuum pump.

$$P = \frac{273.15 \times 10^{10} Vl}{760AT\left(\frac{76p_0}{14.7}\right)}\left(\frac{dp}{dt}\right) \quad (3)$$

In this equation, P, V, l, A, T, p_0 and dp/dt represent the gas permeability (barrer, 1 barrer = 10^{-10} cm^3 (STP) cm cm^{-2} s^{-1} cm Hg^{-1}), the downstream volume (cm^3), the thickness of the membrane selective layer (μm), the active surface area of the membrane (cm^2), the operating temperature (K), the feed pressure (psia) and the steady-state rate of increasing downstream pressure, respectively.

As shown in eqn (4), the ideal selectivity of a pair of gases (A relative to B) was calculated by dividing the pure gas permeability of A by the pure gas permeability of B.

$$\alpha_{A/B} = \frac{P_A}{P_B} \quad (4)$$

A schematic of the gas permeability set-up is presented in Fig. S3.†

Results and discussion

Characterization of NaX nano-zeolites

The XRD patterns of the synthesized NaX and NaX–COOH nano-zeolites are demonstrated in Fig. 1a and evaluated with the standard XRD pattern. As shown in Fig. 1a, the obtained XRD patterns are consistent with the standard XRD pattern and obviously indicate that the synthesized crystals of the zeolites are pure.[20] A mean crystal size of 16 nm was obtained using Scherrer's equation (eqn (1)).

An FESEM image of the synthesized zeolites is presented in Fig. 1b. The FESEM images clearly reveal that the zeolite particles are morphologically alike and the particle size of the synthesized samples is about 40 to 90 nm.

Fig. 1c shows the DLS analysis to determine the particle size distribution of the NaX and NaX–COOH nano-zeolites. As indicated in this figure, the particle size distribution of NaX and NaX–COOH nano-zeolites is in the range of 40 to 90 nm, and the means are 55 and 57 nm, respectively. In addition, the results of the DLS test are in good agreement with the FESEM and XRD results. The crystalline structures of unmodified and modified particles have a uniform distribution.

The FTIR spectra of the NaX and NaX–COOH nano-zeolites are displayed in Fig. 1d. The band at 462 cm^{-1} is attributed to the internal vibrations of TO_4 (T = Si or Al) tetrahedral (S4R symmetric bending), whereas the band at 563 cm^{-1} is related to the double-ring vibration (D6R T–O–T symmetric stretching). The peak at 671 cm^{-1} detects the internal vibration of T–O symmetric stretching, while the peak at 755 cm^{-1} demonstrates vibrations corresponding to external linkages between tetrahedra (S4R T–O–T symmetric stretching). The 986 cm^{-1} band is assigned to the Si–O–Al asymmetric stretching vibration mode of the T–O bonds. The peaks in the wave number range 2500–3800 cm^{-1} and 1647 cm^{-1} indicate O–H stretching of absorbed water in the cavities and channels of NaX zeolite and the O–H bending vibration of water molecules, respectively.[25–27] As can be seen, in the spectrum of the modified zeolite, in addition to the major peaks of the crystal structure, the carboxylic group peaks appear. The peak appearing at 1716 cm^{-1} corresponds to the free carboxylic acid C=O stretch. The wide peak of the O–H band is also shifted to lower wave numbers, which indicates the O–H bond in the carboxylic acid group.

Moreover, the physical properties of nano-zeolites obtained from BET analysis are presented in Table 2. The BET surface area, total pore volume and mean pore size of the NaX nano-zeolite were higher than those of the functionalized zeolite. This reduction is due to the imposition of functional groups into the vacuity of the NaX zeolite micropores, which results in partial blocking of the micropores.[28]

Characterization of membranes

Morphology of membranes. The surface SEM images of the membranes are displayed in Fig. 2 and S4.† It can be seen that the surface of the pure membrane is clean and homogeneous without any pores. The distribution of zeolites on the membrane surface increases with an increase in zeolites up to 2% wt. A suitable dispersion of nano-zeolites and desirable interfacial interaction between the polymer and fillers are observed at each zeolite loading. In addition, the cross-sectional SEM images demonstrate that a moderately dense Pebax-1657 layer was formed on the porous PES support layer without any cracks or defects, as indicated in Fig. 3.

Also, MSL-MMMs containing 0.5 to 1.5% wt NaX and NaX–COOH zeolites reveal that zeolite nanoparticles in the polymeric matrix are uniformly dispersed without any accumulation or interfacial voids, while the modified zeolites had much better

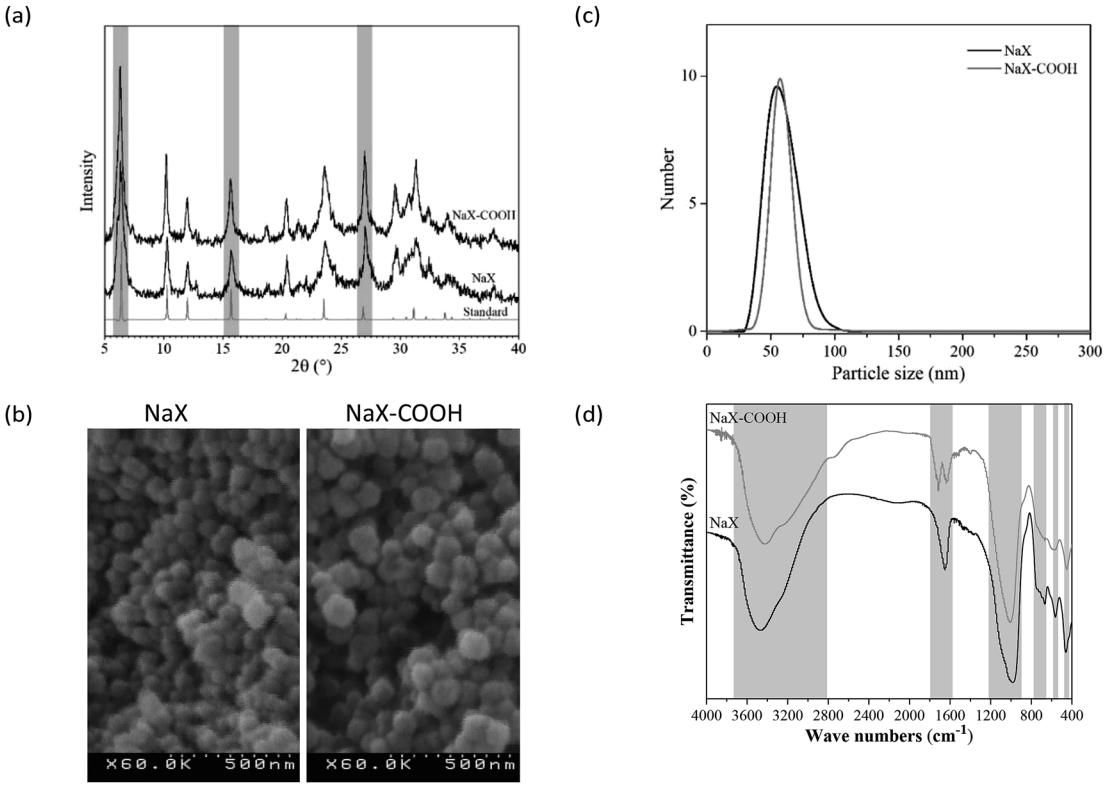

Fig. 1 The XRD patterns (a), FESEM image (b), DLS results (c) and FTIR spectra (d) of the synthesized NaX and NaX–COOH nano-zeolites.

distribution and very suitable interfacial interactions in the matrix. The suitable dispersion is due to the rubbery nature of the polymer phase and the presence of soft segments of PEO in Pebax-1657, while the zeolite particles stick well to the polymer.

At a zeolite loading of 2% wt, the NaX nano-zeolites are approximately agglomerated, while the NaX–COOH nano-zeolites are free of any defects such as non-selective voids at the interface, an agglomeration or sedimentation of particles due to the presence of the carboxylic functional groups and also due to the strong interaction and increase in the stress concentration at the interfaces of the polymer and filler.[16]

Thermal behaviour of membranes. The glass transition temperature (T_g) and crystallinity degree of the membranes are presented in Table 3. It can be seen that the T_g values of MSL-MMMs containing nano-zeolites were higher than that of the neat Pebax-1657 membrane and also an increase in the NaX and NaX–COOH zeolite loading led to an increase in the T_g and total crystallinity. This thermal behavior for the MSL-MMMs is due to an increase in the interfacial interactions and the rigidification of the polymer chains around the nanoparticles.[13] In other words, by incorporating NaX and NaX–COOH fillers into Pebax-1657, the nanoparticles were placed into the free volume between the polymer chains, which restricted the thermal motions of the polymer chains by reducing the frequency and amplitude of the polymer jumping chains. The increases in T_g and crystallinity degree for the membranes filled with the NaX–COOH nano-zeolite were much greater than for the membranes filled with the NaX nano-zeolite due to the presence of carboxylic groups and a stronger interaction with the polymer chains, resulting in greater rigidification of the polymer chains.[17] Also, according to other researchers, the surface modification of nanoparticles with different functional groups increases the T_g and crystallinity degree of the membranes containing modified nanoparticles in comparison to the unmodified nanoparticles.[2,3,16,17]

Table 2 The results of BET analysis of the NaX and NaX–COOH

Sample name	BET surface area ($m^2\ g^{-1}$)	Total pore volume ($cm^3\ g^{-1}$)	Mean pore diameter (nm)
NaX	573	0.350	0.81
NaX–COOH	520	0.322	0.77

Chemical properties of membranes. The FTIR spectra of the neat and MSL-MMMs are presented in Fig. 4. As can be seen, for the neat and MSL-MMMs, the characteristic peak at a wave number of 1094 cm^{-1} is related to the stretching vibration of the C–O–C group in the soft PEO segment and the peaks at 1636, 1730, and 3297 cm^{-1} are ascribed to the stretching vibration of H–N–C=O, O–C=O and N–H bonds in the hard PA6 segment of Pebax-1657.[29]

As indicated in the spectra of the zeolite-filled MSL-MMMs, the intensity of the characteristic peaks at 800–1200, 1500–1800 and 2800–3500 cm^{-1} changed with an increase in the NaX and NaX–COOH zeolite loading of the membranes. The peak at 800–1200 cm^{-1} is associated with an improvement in the interaction of zeolites and the C–O–C group of the soft PEO segment[30,31] and the peaks at 1500–1800 and 2800–3500 cm^{-1}

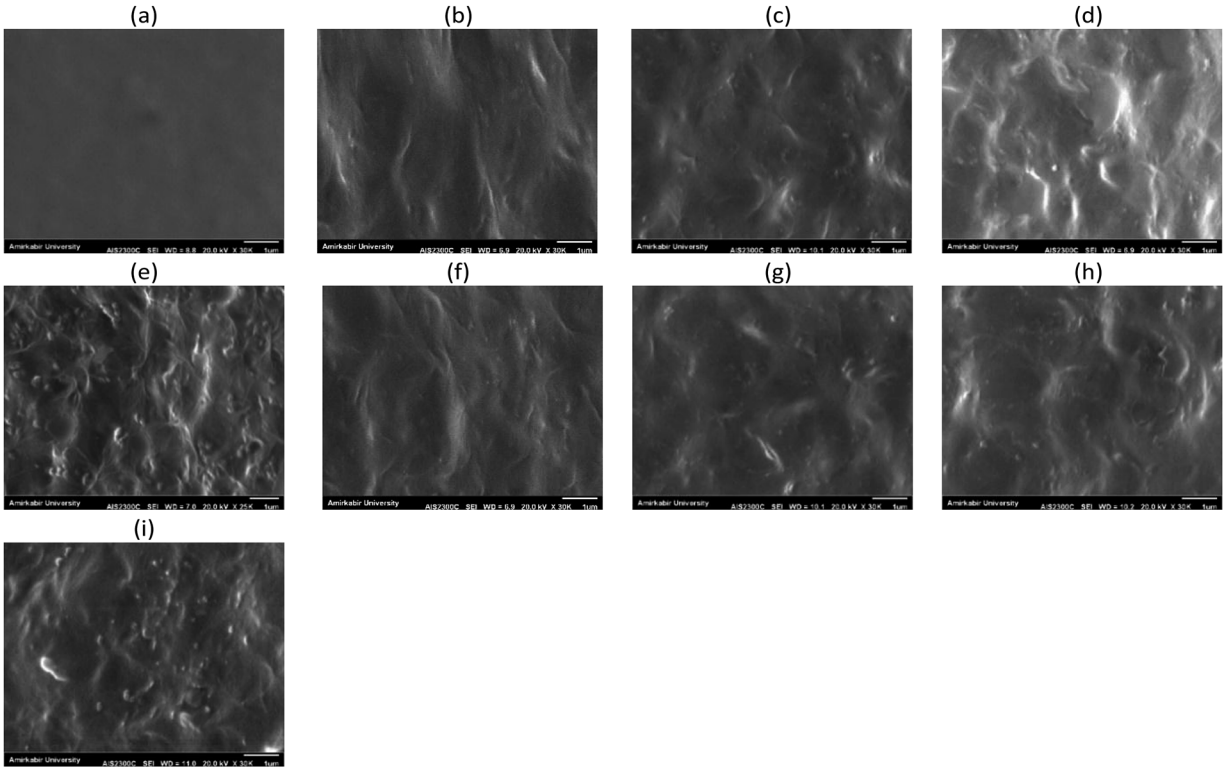

Fig. 2 The SEM surface images of the active layer of PP (a), PPN0.5 (b), PPN1 (c), PPN1.5 (d), PPN2 (e), PPNC0.5 (f), PPNC1 (g), PPNC1.5 (h) and PPNC2 (i).

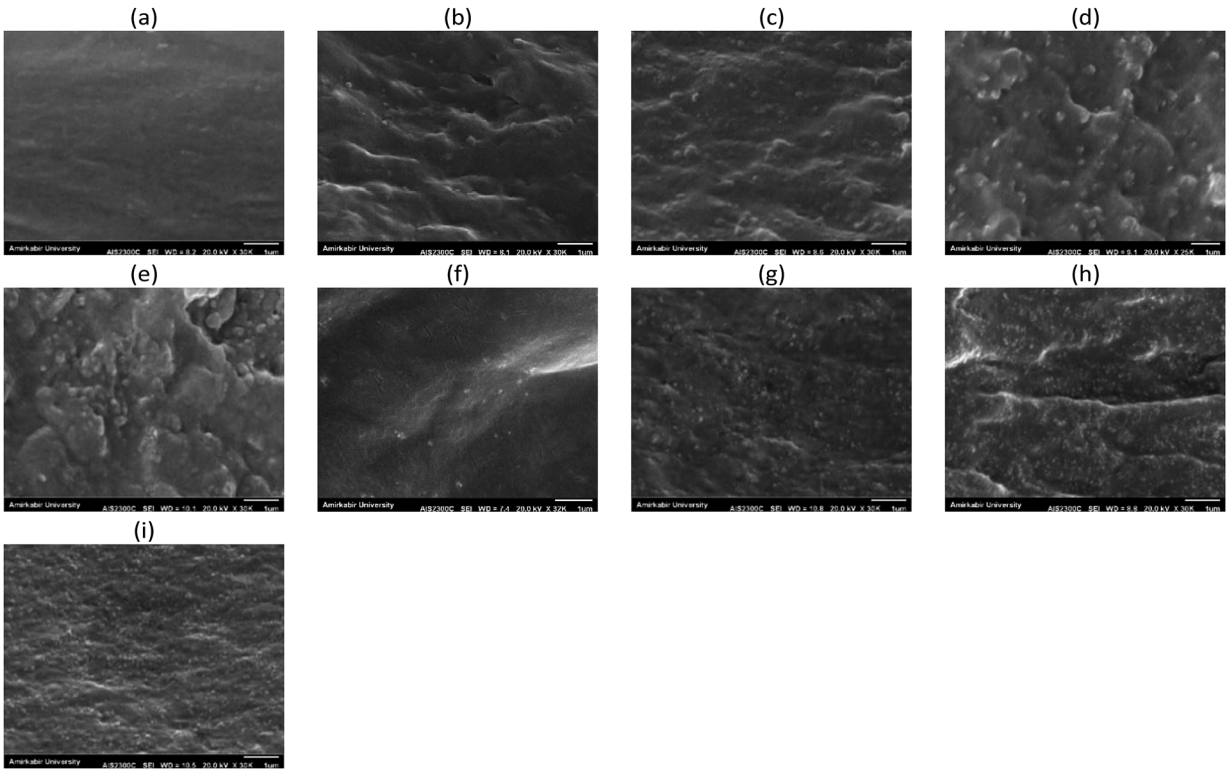

Fig. 3 The SEM cross sectional images of the active layer of PP (a), PPN0.5 (b), PPN1 (c), PPN1.5 (d), PPN2 (e), PPNC0.5 (f), PPNC1 (g), PPNC1.5 (h) and PPNC2 (i).

Table 3 The glass transition temperature and degree of crystallinity of the membranes

		ΔH_m (J g^{-1})		$X_{crystallinity}$ (%)		
Sample name	T_g (°C)	PEO	PA	PEO	PA	Total
PP	−55.35	14.43	23.07	14.45	25.08	18.7
PPN0.5	−52.99	16.32	23.35	16.35	25.38	19.96
PPN1	−51.45	18.25	23.87	18.28	25.95	21.35
PPN1.5	−49.38	19.54	24.68	19.57	26.83	22.47
PPN2	−48.52	20.93	25.71	20.96	27.95	23.76
PPNC0.5	−52.66	17.11	23.41	17.14	25.45	20.46
PPNC1	−49.41	19.34	25.13	19.37	27.32	22.55
PPNC1.5	−47.04	20.87	26.91	20.9	29.25	24.24
PPNC2	−46.13	22.41	27.73	22.44	30.14	25.52

are attributed to the interaction of zeolites and N–H, H–N–C=O and O–C=O groups of the hard PA6 segment. The broad band appearing at a wave number of 3500 cm^{-1} is due to the formation of hydrogen bonding between the zeolites and the polymer matrix.[32,33] These results are in good agreement with the observations reported in other investigations[30,32] and the results of the DSC analysis.

Hydrophilic properties of membranes. The contact angle test was used to investigate the changes in the membrane hydrophilicity. Table 4 shows the results of water contact angle analysis for the neat membrane and MSL-MMMs. As can be seen, the contact angle for the neat membrane was 64°, which decreased with an increase in the loading of NaX and NaX–COOH nano-zeolites into the polymeric matrix. The reason is that the NaX zeolite is known to be a highly hydrophilic filler, so loading it into the membranes increases the hydrophilicity of the mixed matrix membranes.[31]

On the other hand, the presence of carboxylate groups in the membrane leads to an increase in membrane hydrophilicity.[19]

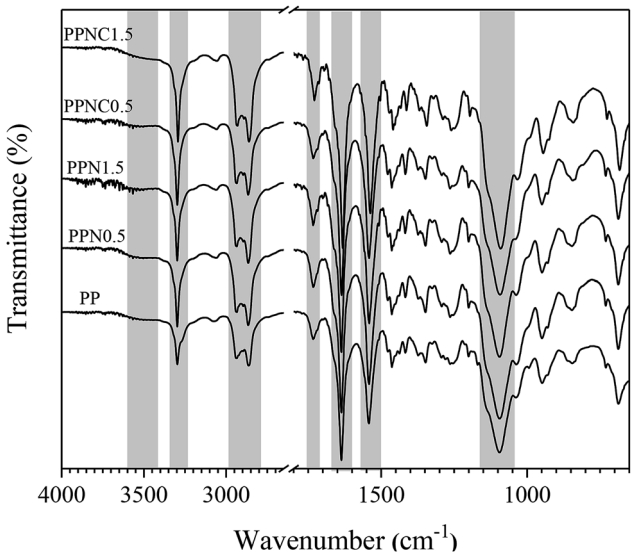

Fig. 4 The FTIR spectra of the fabricated neat membrane and MSL-MMMs.

Table 4 The water contact angle of the neat membrane and MSL-MMMs

Membrane sample	Contact angle (°)
PP	64
PPN0.5	63
PPN1	61
PPN1.5	59
PPN2	55
PPNC0.5	62
PPNC1	59
PPNC1.5	57
PPNC2	54

Therefore, at a lower loading, the carboxylic group increases the hydrophilicity of the MSL-MMMs containing modified zeolite compared to membranes containing the unmodified zeolite. The contact angle results were in good agreement with the contact angle data in previous studies.[30,31]

Gas permeation of membranes

Effect of nanoparticles loading. In order to investigate the role of surface modification of the NaX nano-zeolite with a carboxylic functional group, a gas permeation analysis of the MSL-MMMs comprising NaX and NaX–COOH was performed at 25 °C and 6 bar. The pure permeability behaviour of N_2 (critical temperature (T_c) = 126.2 K, kinetic diameter (D_k) = 3.64 Å), CH_4 (T_c = 190.8 K, D_k = 3.8 Å) and CO_2 (T_c = 304.2 K, D_k = 3.3 Å) gases and the ideal selectivity of CO_2/CH_4, CH_4/N_2 and CO_2/N_2 for the fabricated membranes are shown in Fig. 5. The gas permeability behaviors can be justified by the solution-diffusion model for the dense polymeric membranes. In this model, the solubility and diffusivity of gases both play an important role in the transport of gases through the membranes.

In MSL-MMMs, the solubility of gases can be affected by the condensability of the gases (the critical temperature of gases), the interactions between the gases and polymer chains, and interactions between the gases and the functional groups of the nanoparticles. Likewise, the diffusivity of the gases can be affected by the kinetic diameter of the gases, the partial fractional free volume of the polymer, interactions between polymer and gases, polymer chain flexibility, nanoparticle pore size, pore blocking of nanoparticles, compatibility of the nanoparticles and the polymer, and agglomeration of nanoparticles. The presence of nanoparticles in the polymeric matrix has a variety of effects on the morphology and performance of MSL-MMMs. The solubility of the polar gases and the molecular sieving of the small kinetic diameter gases increase. The tortuousness of the permeation pathway increases for non-polar penetrant molecules and for gases larger than the filler pores. The strong compatibility and interaction between the polymer and filler lead to a hardening of the polymer chains around the polymer/filler interface and, occasionally, to partial pore blocking of the particles. The placement of the fillers between the chains leads to a reduction in movement and flexibility of the chains and fractional free volume.

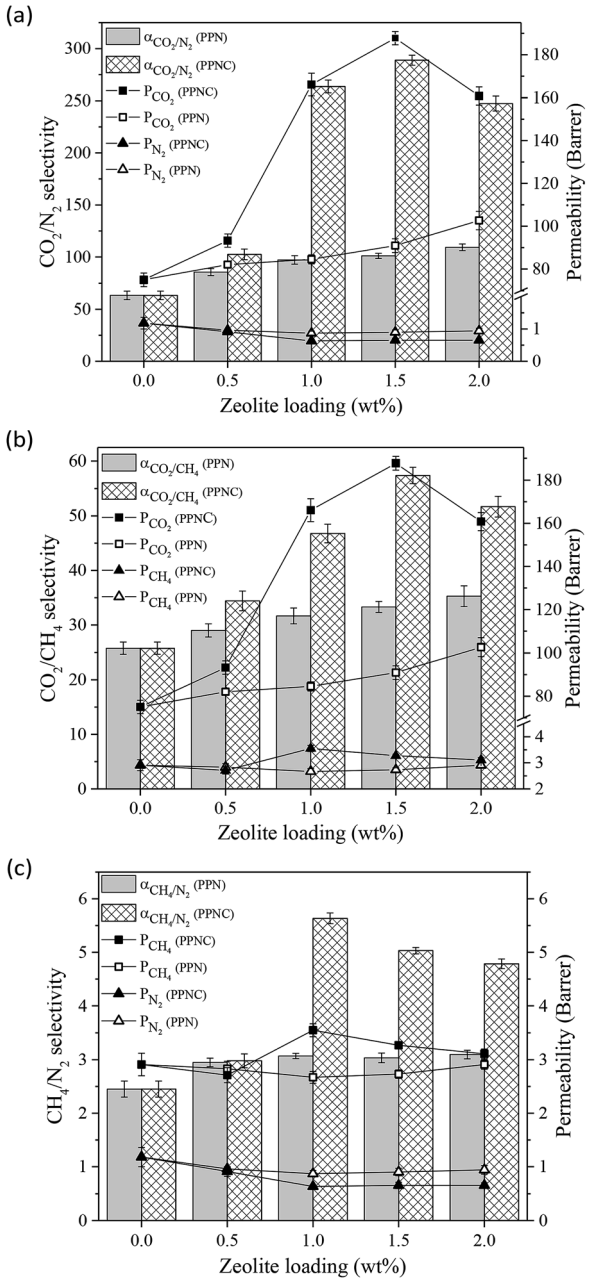

Fig. 5 The effect of nano-zeolite loading on the gas permeability and selectivity of the CO_2 and N_2 mixture (a), CO_2 and CH_4 mixture (b) and CH_4 and N_2 mixture (c) at 6 bar and 25 °C.

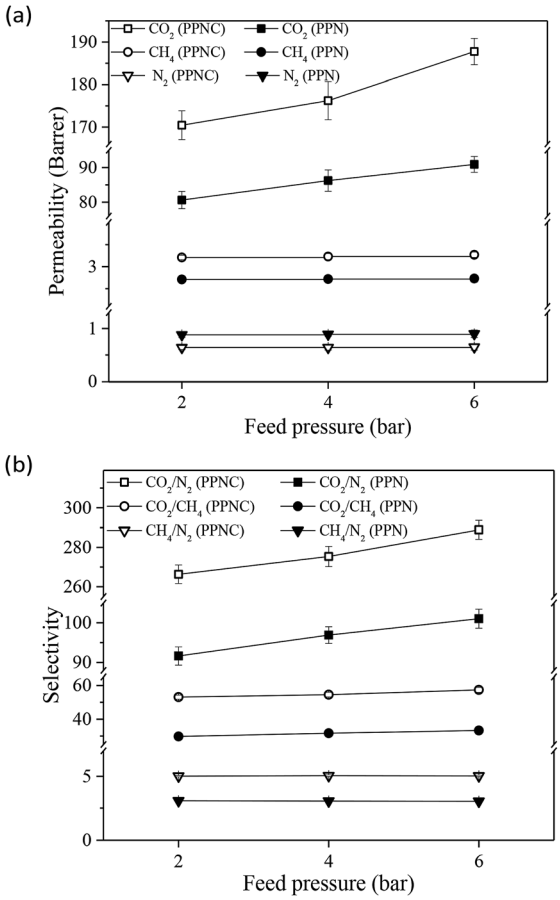

Fig. 6 The effect of operating pressure on the gas permeability (a) and selectivity (b) of the PPN1.5 and PPNC1.5 at 25 °C.

As shown in Fig. 5, for all the fabricated membranes, the CO_2 permeability was significantly higher than for CH_4 or N_2 gases. The much higher critical temperature and the smaller kinetic diameter of CO_2 than for the other gases caused greater solubility and diffusivity. In addition, CO_2 polar gas has the highest solubility due to the strong tendency towards the polar segment of Pebax-1657 compared to the non-polar gases (CH_4 and N_2). Zeolites with a low tendency to absorb CH_4 and N_2 gases also lead to prolongation of the total path of their penetration into the membrane. It should be noted that the pore size of the zeolites is larger than the molecular size of all the tested gases, but the zeolites actually separate gases by selective sorption, and the pore flow through the zeolite cavities has a smaller effect on separation. Therefore, the higher solubility and higher diffusion of the CO_2 gas resulted in a higher permeability of this gas compared to other gases through the neat membrane and MSL-MMMs.

As shown in Fig. 5, the combination of NaX and NaX–COOH porous nano-fillers significantly affected the permeability and selectivity. By increasing the amount of nanoparticle loading up to 1.5% wt, the permeability of CO_2 gas increased, but the permeability of other gases was reduced. Likewise, the selectivity of all pairs of gases increased. The SEM surface images of the MSL-MMMs in Fig. 2 showed that by increasing the loading amount of nano-zeolites, the number of these fillers increases on the membrane surface. Therefore, due to the high sorption capacity of the zeolite filler for polar gases and the high chemical tendency of CO_2 with the NaX nano-zeolites, the interaction between the gas and membrane surface increased and led to an increase in CO_2 permeability. On the other hand, the gradual decrease in the permeability of the other gases could be due to the formation of a hard layer around the nano-fillers, a decrease in the fractional free volume, partial pore blocking of the nanoparticles and, most importantly, the weak tendency of zeolites towards non-polar gases.[4,9]

Table 5 Comparison of the gas separation performance of the MMMs based on Pebax containing different modified fillers

Filler type	Filler loading[a] (% wt)	P (bar)	T (°C)	Permeability (barrer)			Selectivity			References
				CO_2	CH_4	N_2	CO_2/N_2	CO_2/CH_4	CH_4/N_2	
NaX–COOH	15	6	25	187.76	3.27	0.65	288.86	57.41	5.03	This work
SiO_2–COOH	8	2	25	133.01	2.96	1.08	123.16	45	2.74	10
MWNTs-NH_2	9	7	35	200	12.5	3.84	52	16	3.26	14
GO-DA-Zn^{2+}	1	2	30	137.9	4.79	—	—	28.8	—	38
UiO-66-NH_2	10	3	25	87	—	1.32	66	—	—	12
ImGO	0.8	8	25	76.20	2.5	0.72	105.50	30.5	3.47	2
UiO-66-NH_2	15	7	25	393.4	9.9	—	—	39.8	—	16
TiO_2-CMC	3	20	25	194.6	—	2.36	82.4	—	—	39
TiO_2-AS	3	20	25	188.6	—	2.22	84.9	—	—	39
GO-IL-NH_2	10	4	25	143	6.25	1.8	79.44	22.88	3.47	40
MIL-53-NH_2	10	10	35	149.1	7.3	2.7	55.22	20.42	2.7	41
GO-APTS	0.7	2	35	172	10.1	3.8	45.26	17.03	2.65	42
ZIF-8-ZN/Ni	10	5	25	408	7.87	—	51.8	—	—	43

[a] Based on the polymer weight.

In the MSL-MMMs comprising NaX–COOH compared to the MSL-MMMs containing NaX, the permeability of CO_2 was much higher and the permeability of CH_4 and N_2 gases was lower. The –COOH functional group of the modified zeolites can effectively enhance the surface affinity toward CO_2 molecules,[34] and as a result, the CO_2 gas permeability and subsequently the CO_2/CH_4 and CO_2/N_2 selectivities increase. In addition, the results of the BET analysis indicated that the smaller pore size of the NaX–COOH compared to the NaX nano-zeolites hinders the permeation of molecules with a high kinetic diameter that would have an effect of improving the CO_2 permeability compared to N_2 and CH_4.[16,28] The merging of nano-zeolite into the Pebax-1657 matrix limits the movement of the polymer chains through the formation of hydrogen bonds between the hydroxyl groups of the filler and the Pebax-1657 polymer chains, as illustrated by the FTIR analysis in Fig. 4. This limitation is greater for the modified zeolites due to the formation of stronger bonds, but the solubility of polar gases is also significantly increased. Based on the results of the DSC test in Table 3, the addition of nano-zeolites made the polymeric chains harder. Thus MSL-MMMs containing NaX–COOH and NaX have a significantly higher T_g than the neat membranes.

With a loading of 2% wt of unmodified NaX zeolite, the nanoparticle aggregation tendency increased, as shown in Fig. 5. The weak interactions and the lack of appropriate adhesion between the filler and the polymer caused the accumulation of nanoparticles. However, the CO_2 permeability decreased dramatically for the MSL-MMM with the maximum modified zeolite loading (2% wt). Reducing the CO_2 permeability at the highest loading amount of NaX–COOH can be attributed to the increased interaction between the polymer and the functionalized filler. Thus, the filler affects the crystallinity of polyamide and polyethylene oxide segments. The presence of NaX–COOH in the PEO soft section leads to a hardening of the chains and thus reduces the CO_2 gas permeability; although in the polyamide sector, it leads to the breakdown of the amide chain and a slight increase in the free volume, as proven by the FTIR and DSC analyses.

Fig. 5 shows the ideal selectivity of the pairs of gases for the neat membrane and MSL-MMMs. For the neat membrane, the CO_2/N_2, CO_2/CH_4 and CH_4/N_2 ideal selectivities are 63.85, 28.21 and 2.26, respectively. While the addition of NaX and NaX–COOH nano-zeolites resulted in a significant improvement in the ideal selectivity of all pairs of gases. By increasing the loading amount of nano-zeolites to 1.5% wt, the selectivities of CO_2/N_2, CO_2/CH_4 and CH_4/N_2 for the MSL-MMM containing NaX nano-zeolite increased to 101.03, 33.31 and 3.03, respectively, and for the MSL-MMM containing NaX–COOH nano-zeolite they increased to 288.86, 57.42 and 5.03. This trend for gas-pair selectivity can be attributed to their permeability ratio, and the reasons for the permeability behaviour are expressed above.

Effect of operating pressure. The effect of operating pressure on the gas permeability and ideal selectivity of the MSL-MMMs containing 1.5% wt of NaX and NaX–COOH nano-fillers were investigated and are shown in Fig. 6. It can be observed that the permeability of all tested gases for the prepared membranes increased as the pressure changed from 2 to 6 bar, while the CO_2 permeability increase was significantly higher compared to CH_4 and N_2. The observed behavior for CO_2 permeability with increasing operating pressure is consistent with the results reported in the literature for rubbery membranes.[35,36] In general, the operating pressure has a significant effect on the sorption of condensable gases like CO_2 into the rubbery membranes, so that the gas sorption increases with an increase in the operating pressure. The sorption of condensable CO_2 molecules into the membranes leads to an increase in the mobility of the polymeric chains, and a greater fractional free volume was produced in the MSL-MMM,[37] consequently enhancing the CO_2 diffusivity in the MSL-MMMs. Additionally, by applying a higher pressure, the CO_2 sorption by zeolite fillers in the MSL-MMMs is intensified, which results in enhancement of CO_2 permeability. Ultimately, the enhancement in the CO_2 sorption and diffusion in the MSL-

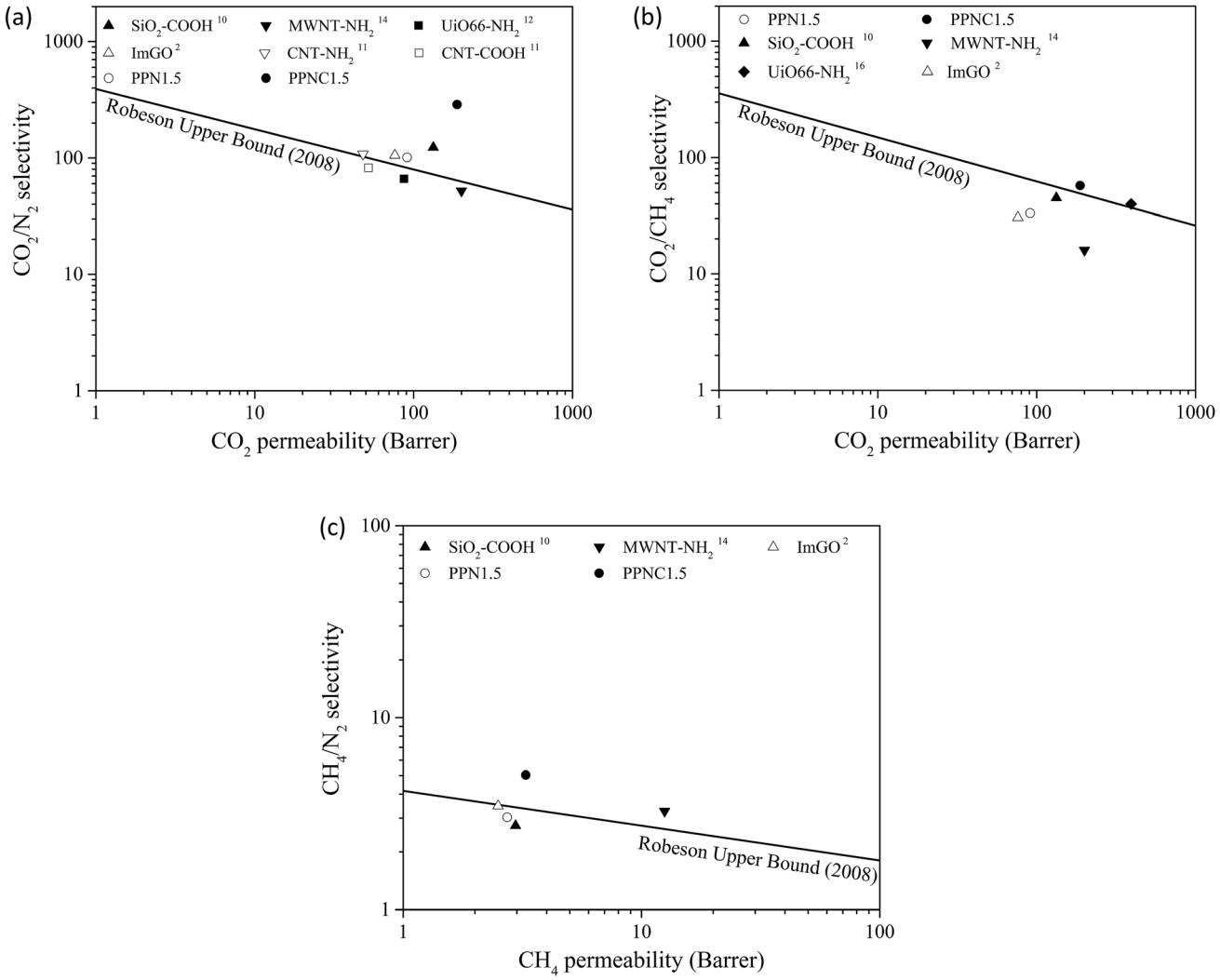

Fig. 7 Comparison of the performance of various MMMs for the separation of CO_2/N_2, CO_2/CH_4 and CH_4/N_2 mixtures with Robeson's upper bound.

MMMs with higher operating pressure leads to higher CO_2 permeability.

As shown in Fig. 6a, the permeability of CH_4 and N_2 gases appears to be constant with the application of higher pressure. This behavior implies that the fabricated membranes are not compacted with increasing operating pressure. The prepared membranes based on Pebax-1657 have a semi-crystalline structure, in which the crystalline parts, such as rigid segments and physical crosslinking in the membrane structure, can provide the mechanical strength. Thus, resistance *versus* compaction and reducing the movement of the polymer chains are observed with an increase in feed pressure. Additionally, incorporation of nanoparticles increases the mechanical strength of MSL-MMMs. The effect of modified nanoparticles was greater than that of the unmodified nanoparticles in increasing the mechanical strength. Ultimately, with an increase in the operating pressure, the mass transfer driving force increases and causes an increase in the gas diffusivity. Therefore, the permeability of gases increases very slightly, with no compaction occurring in the membranes and an increase in gas diffusivity. The gas permeability increase in interacting and polar gases like CO_2 in the MSL-MMMs including modified nano-zeolites was more significant due to the presence of carboxylic functional groups. Furthermore, the CO_2/N_2 and CO_2/CH_4 selectivities were slightly enhanced as the operating pressure increased, while the CH_4/N_2 selectivity was almost constant, as shown in Fig. 6b. These trends can be attributed to the effect of operating pressure on the gas permeabilities of the prepared MSL-MMMs. Similar observations have been reported in previous research.[2,16,30]

Stability of MSL-MMMs in long-term operation. In order to verify the stability of the MSL-MMMs, a long-term permeation test for the pure gases CO_2, CH_4 and N_2 was performed for two PPN1.5 and PPNCC1.5 membrane samples. The stability analysis was carried out for 50 h. Fig. S5† shows the CO_2 permeability and the selectivity of CO_2/N_2 and CO_2/CH_4 as a function of operating time at 6 bar and 25 °C. As can be seen in this figure, for both MSL-MMMs, the permeabilities and selectivities

were somewhat stable and no declining tendency was observed. These behaviors show that there is no competitive effect between the tested gases, and plasticization and compaction of the prepared MMMS did not occur. Consequently, by applying higher pressure or long-term permeation, the non-polar gases remain unchanged. The stability of the MSL-MMMs means that these membranes are promising for CO_2 capture in industrial applications.

Comparison with other studies. The gas separation performance of the MMMs is different because of different membrane fabrication conditions, as well as different operating conditions for the gas permeability measurement. Many factors affect the permeability and selectivity of MMMs based on the Pebax polymer, but the most important of these factors are operating temperature, feed pressure, gas permeation module, effective membrane surface, selective membrane layer thickness, type and concentration of Pebax, Pebax solvent, and type and morphology of the filler. In order to compare the permeability and selectivity of MMMs, one of the most important factors is the type of nanoparticle used as the filler in a polymeric matrix. A variety of pure and functionalized nanoparticles have been widely used by researchers and different results have been reported, some of which are presented in Table 5. By comparing the performances of various MMMs based on Pebax-1657, it is found that the CO_2/N_2 and CO_2/CH_4 selectivities of the MSL-MMM containing 1.5% wt of NaX zeolite are higher than the selectivity of MMMs provided by other researchers. In addition, the CO_2 permeability and CO_2/N_2 selectivity of the MSL-MMM containing 1.5% wt of NaX–COOH nano-zeolite are surprising. It can be seen in Table 5 that the modification of nanoparticles with various functional groups, such as amine and carboxyl, has a significant effect on the permeability and selectivity of the membranes.

Finally, the permselectivities of the MSL-MMMs were compared with Robeson's upper limit and the results are shown in Fig. 7. As can be seen, the PPN1.5 and PPNC1.5 membranes overcome Robeson's upper bound, which proves that the efficiency of separation is much higher than that of conventional MMMs in other research.

Conclusions

A highly permeable and highly selective membrane including the zeolites combined with a Pebax-1657 moderate selective layer on a highly permeable PES support layer was developed for gas separation applications. Functionalized NaX nano-zeolites were employed to comprehend the effect of chemical surface modification on the gas separation performance compared to conventional MMMs. Loading the NaX and NaX–COOH nano-zeolites into a Pebax polymeric matrix effectively promoted the CO_2 permeability and CO_2/N_2, CO_2/CH_4 and N_2/CH_4 selectivities due to the better CO_2 sorption, good compatibility and strong interfacial interaction of the filler/polymer chains. In addition, the permeability and selectivity of MSL-MMMs were amplified by changing the operating pressure from 2 to 6 bar. The results confirmed that MSL-MMMs containing carboxyl modified NaX zeolite had superior separation performance compared to MSL-MMMs containing neat NaX zeolite. Moreover, SEM images indicated that the modification of NaX nano-zeolite led to good filler/polymer interaction and filler dispersion. The MSL-MMMs were also explored by performing DSC, FTIR and long-term permeability tests. The results revealed that the addition of nano-zeolites rigidified the polymer matrix chains by forming strong hydrogen bonds, ultimately preventing the occurrence of compaction and plasticization of MSL-MMMs. MSL-MMMs containing 1.5% wt of carboxyl functionalized NaX nanoparticles passed the Robeson's upper bound limit for the separation of CO_2/N_2, CO_2/CH_4 and CH_4/N_2. Finally, it can be deduced that loading functionalized NaX into the Pebax-1657 moderate selective layer is feasible for developing MSL-MMMs with high separation performance in the cases of CO_2 in flue and natural gas.

Conflicts of interest

There are no conflicts to declare.

References

1 G. Dong, H. Li and V. Chen, *J. Mater. Chem. A*, 2013, **1**, 4610.
2 Y. Dai, X. Ruan, Z. Yan, K. Yang, M. Yu, H. Li, W. Zhao and G. He, *Sep. Purif. Technol.*, 2016, **166**, 171–180.
3 H. Wu, X. Li, Y. Li, S. Wang, R. Guo, Z. Jiang, C. Wu, Q. Xin and X. Lu, *J. Membr. Sci.*, 2014, **465**, 78–90.
4 N. Kosinov, J. Gascon, F. Kapteijn and E. J. J. J. o. M. S. Hensen, *J. Membr. Sci.*, 2016, **499**, 65–79.
5 M. A. Aroon, A. F. Ismail, T. Matsuura and M. M. Montazer-Rahmati, *Sep. Purif. Technol.*, 2010, **75**, 229–242.
6 T.-S. Chung, L. Y. Jiang, Y. Li and S. Kulprathipanja, *Prog. Polym. Sci.*, 2007, **32**, 483–507.
7 P. S. Goh, A. F. Ismail, S. M. Sanip, B. C. Ng and M. Aziz, *Sep. Purif. Technol.*, 2011, **81**, 243–264.
8 D. Zhao, J. Ren, Y. Wang, Y. Qiu, H. Li, K. Hua, X. Li, J. Ji and M. Deng, *J. Membr. Sci.*, 2017, **521**, 104–113.
9 Y. Cheng, Z. Wang and D. Zhao, *Ind. Eng. Chem. Res.*, 2018, **57**, 4139–4169.
10 A. Ghadimi, T. Mohammadi and N. Kasiri, *Int. J. Hydrogen Energy*, 2015, **40**, 9723–9732.
11 S. A. Habibiannejad, A. Aroujalian and A. Raisi, *RSC Adv.*, 2016, **6**, 79563–79577.
12 J. Shen, G. Liu, K. Huang, Q. Li, K. Guan, Y. Li and W. Jin, *J. Membr. Sci.*, 2016, **513**, 155–165.
13 N. C. Su, H. G. Buss, B. D. McCloskey and J. J. Urban, *ACS Macro Lett.*, 2015, **4**, 1239–1243.
14 D. Zhao, J. Ren, H. Li, X. Li and M. Deng, *J. Membr. Sci.*, 2014, **467**, 41–47.
15 H. R. Amedi and M. Aghajani, *Microporous Mesoporous Mater.*, 2017, **247**, 124–135.
16 M. Mozafari, R. Abedini and A. Rahimpour, *J. Mater. Chem. A*, 2018, **6**, 12380–12392.
17 P. D. Sutrisna, J. Hou, M. Y. Zulkifli, H. Li, Y. Zhang, W. Liang, D. M. D'Alessandro and V. Chen, *J. Mater. Chem. A*, 2018, **6**, 918–931.

18 X. Jiang, S. Li, S. He, Y. Bai and L. Shao, *J. Mater. Chem. A*, 2018, **6**, 15064–15073.
19 J. Shen, L. Wu, D. Wang and C. Gao, *Desalination*, 2008, **223**, 425–437.
20 M. Ansari, A. Aroujalian, A. Raisi, B. Dabir and M. Fathizadeh, *Adv. Powder Technol.*, 2014, **25**, 722–727.
21 P. G. Ingole, M. I. Baig, W. K. Choi and H. K. Lee, *J. Mater. Chem. A*, 2016, **4**, 5592–5604.
22 I. Sadeghi, A. Aroujalian, A. Raisi, B. Dabir and M. Fathizadeh, *J. Membr. Sci.*, 2013, **430**, 24–36.
23 A. Ghadimi, M. Amirilargani, T. Mohammadi, N. Kasiri and B. Sadatnia, *J. Membr. Sci.*, 2014, **458**, 14–26.
24 H. Rabiee, A. Ghadimi and T. Mohammadi, *J. Membr. Sci.*, 2015, **476**, 286–302.
25 J. Coates, *Encyclopedia of analytical chemistry*, 2000.
26 B. M. Abu-Zied, *Microporous Mesoporous Mater.*, 2011, **139**, 59–66.
27 A. Zainal Abidin, N. H. H. Abu Bakar, E. P. Ng and W. L. Tan, *J. Taibah Univ. Sci.*, 2017, **11**, 1070–1079.
28 X. Wang, H. Li and X.-J. Hou, *J. Phys. Chem. C*, 2012, **116**, 19814–19821.
29 G. Dong, J. Hou, J. Wang, Y. Zhang, V. Chen and J. Liu, *J. Membr. Sci.*, 2016, **520**, 860–868.
30 K. Zarshenas, A. Raisi and A. Aroujalian, *J. Membr. Sci.*, 2016, **510**, 270–283.
31 M. Fathizadeh, A. Aroujalian and A. Raisi, *J. Membr. Sci.*, 2011, **375**, 88–95.
32 R. Surya Murali, A. F. Ismail, M. A. Rahman and S. Sridhar, *Sep. Purif. Technol.*, 2014, **129**, 1–8.
33 L. Xiang, Y. Pan, G. Zeng, J. Jiang, J. Chen and C. Wang, *J. Membr. Sci.*, 2016, **500**, 66–75.
34 B. Liu, H. Li, X. Ma, R. Chen, S. Wang and L. Li, *RSC Adv.*, 2018, **8**, 38965–38973.
35 Y. Naito, Y. Kamiya, K. Terada, K. Mizoguchi and J. S. Wang, *J. Appl. Polym. Sci.*, 1996, **61**, 945–950.
36 H. Lin and B. D. Freeman, *J. Membr. Sci.*, 2004, **239**, 105–117.
37 S. Semenova, S. Smirnov and H. Ohya, *J. Membr. Sci.*, 2000, **172**, 75–89.
38 D. Peng, S. Wang, Z. Tian, X. Wu, Y. Wu, H. Wu, Q. Xin, J. Chen, X. Cao and Z. Jiang, *J. Membr. Sci.*, 2017, **522**, 351–362.
39 A. A. Shamsabadi, F. Seidi, E. Salehi, M. Nozari, A. Rahimpour and M. Soroush, *J. Mater. Chem. A*, 2017, **5**, 4011–4025.
40 G. Huang, A. P. Isfahani, A. Muchtar, K. Sakurai, B. B. Shrestha, D. Qin, D. Yamaguchi, E. Sivaniah and B. Ghalei, *J. Membr. Sci.*, 2018, **565**, 370–379.
41 S. Meshkat, S. Kaliaguine and D. J. S. Rodrigue, *Sep. Purif. Technol.*, 2018, **200**, 177–190.
42 J. Zhang, Q. Xin, X. Li, M. Yun, R. Xu, S. Wang, Y. Li, L. Lin, X. Ding and H. Ye, *J. Membr. Sci.*, 2019, **570**, 343–354.
43 X. Zhang, T. Zhang, Y. Wang, J. Li, C. Liu, N. Li and J. Liao, *J. Membr. Sci.*, 2018, **560**, 38–46.